CHAPTER V - STATIC FRACTURE ANALYSIS OF CONCRETE STRUCTURES

5.1 Introduction

In Chapter IV, the implementation of the crack model (subprogram) on simple pure-tension specimens was preliminarily validated. These pure-tension members are only subject to the mode I fracture response and the directions of crack propagation are fixed and *a priori* known. Thus a fixed, single-crack model can be accurately employed to simulate the fracture behaviour. The validation exercise is extended in this chapter to mode I and mixed-mode fracture simulation of more complicated concrete structures, such as a three-point, single-notched, centrally loaded beam and a four-point, single-notched shear beam.

A three-point, single-notched, centrally loaded beam is first adopted to benchmark the proposed bilinear mode I tensile softening diagram and the related numerical implementation. The specimen is mode I dominant because no shear fracture deformation would occur in this specimen due to the symmetry of the geometry and the loading conditions. Therefore, a fixed, single-crack model is sufficient to simulate the fracture process in such a specimen.

A well-investigated, single-notched shear beam under four-point, mixed-mode static loading conditions is further used to validate the crack model adopted with study of the fracture parameters.

Mesh objectivity is definitely both a requirement and a necessity for any crack model proposed for finite element (FE) fracture analysis in any sensible fracture evaluation of concrete structures. For this reason, three differently meshed FE models of the same geometry were considered to test the objectivity regarding the mesh discretization of the crack model adopted and the numerical technique developed.

All the models of the following three verification problems employ plane stress, and are four-noded and four-Gauss point isoparametric elements, with the exception of the second-order, eight-noded nine-Gauss point isoparametric elements used in case 3 for the

validation of the crack models and the implementation on second-order elements. A modified Newton-Raphson solution procedure is adopted.

5.2 Case 1: three-point, centre-loaded, single-notched beam

A symmetrical centre-notched concrete beam under three-point bending (two supports and a midpoint load) is used to validate the implementation of the cracking model with a parametric study. The beam has a length of 838 mm, a span of 788 mm and a cross-section of 102 mm x 102 mm. The notch:depth ratio (a/d) is 0.5. Malvar & Fourney (1990) carried out 12 experimental tests and also a numerical simulation on the beam.

The beam is symmetrical along its centreline so that only half the beam (as modeled by Malvar & Fourney 1990) needs to be modelled in the FE analysis, as shown in Figure 5.1. The material properties used are as follows:

Young's modulus E = 21 700 MPa; Tensile strength f_t = 3.1 MPa
Poisson's ratio υ = 0.2; Fracture energy G_f = 0.0763 N/mm
Crack characteristic length h_c = 10 mm (width of element at the crack)

Linear, bilinear and non-linear exponential strain-softening branches are used to investigate the cracking behaviour of the beam, as shown in Figure 5.2. This symmetrical specimen is not sensitive to shear softening since the crack propagates along the centre of the beam. No shear deformation would occur in the crack formation zone. Numerical studies are compared with the experimental results from Malvar & Fourney (1990), as shown in Figure 5.3.

Cornelissen *et al.* (1986) conducted a series of tests to determine the crack-softening characteristics of normal-weight concrete and proposed an empirical formula obtained by curve fitting the test data:

$$\frac{\sigma}{f_t} = \left[1 + (C_1 \frac{\delta}{\delta_0})^3\right] e^{(-C_2 \frac{\delta}{\delta_0})} - \frac{\delta}{\delta_0}(1 + C_1^3) e^{(-C_2)} \qquad (5.1)$$

Where $C_1 = 3$, $C_2 = 6.93$, δ is the crack opening and δ_0 is the crack opening at which the crack stress can no longer be transferred. This stress-crack opening relationship in equation (5.1) is transformed into a crack stress-strain law for this study, as shown in Figure 5.2.

As shown in Figure 5.3, the calculated linear softening response (labelled as LS) yields the highest peak loading of all the softening relationships. This indicates that if linear softening is assumed when concrete fracture is modelled, then the resistance of the structure will be overestimated. The calculated non-linear softening response based on the experimental softening relationship derived by Cornelissen *et al.* (1986) (labelled as CS), yields the closest load-displacement relationship to the experimental results.

The bilinear softening models (labelled as BLS) improve the response significantly when compared with the linear softening model. Therefore, the bilinear softening model is able to provide a reasonably accurate prediction of the cracking response, while remaining relatively simple to implement. The investigation demonstrates the importance of adopting bilinear softening analysis in concrete structures, instead of the general application of linear softening in concrete cracking analysis used in the past. Although Cornelissen *et al.*'s exponential non-linear softening relationship remains the most accurate, it requires greater effort to implement in an FE analysis compared with the simpler bilinear softening model.

A series of constitutive parameters for bilinear softening curves was investigated for the purpose of calibrating the correct range of shape parameters α_1 and α_2 for concrete structures.

A parameter study was conducted to determine the bilinear softening model parameters α_1 and α_2 that best fit the experimental response. The results of the parameter study are shown in Figures 5.2 to 5.7, in which it can be seen that by setting the bilinear shape parameters α_1 to between 1/3 and 0.44 and α_2 to 0.1 respectively, good agreement with the experimental results can be obtained.

By selecting α_2 as constant and equal to 0.1, and setting α_1 to 0.25, 1/3 and 0.44, it can be seen that the first part of the bilinear softening modulus becomes steeper as α_1 increases (see Figure 5.2), while the predicted response improves when compared with the experimental results (Figure 5.3).

From Figures 5.5 and 5.7, in which α_1 is fixed at 0.25 and 1/3 respectively (see Figures 5.4 and 5.6), while α_2 is varied from 0.1 to 0.3, it can be seen that as α_2 decreases from 0.3 to 0.1, the first part of the bilinear softening modulus becomes steeper and the second part of the bilinear softening branch becomes flattener (see Figures 5.4 and 5.6), while the predicted response improves. It is concluded that the first part of the bilinear softening modulus is of greater importance than the second part, although it is the combination of the bilinear shape parameters α_1 and α_2 that determines the complete softening response. It is important to note that the particular values of α_1 and α_2 would depend on the concrete mix of the particular structure and need to be carefully determined experimentally.

Compared with the numerical investigation by Malvar & Fourney (1990), this study has produced a better simulation of the experiment results.

It is evident that the cracking model and the calculation procedure can accurately predict the cracking behaviour of concrete, provided a suitable softening response is adopted.

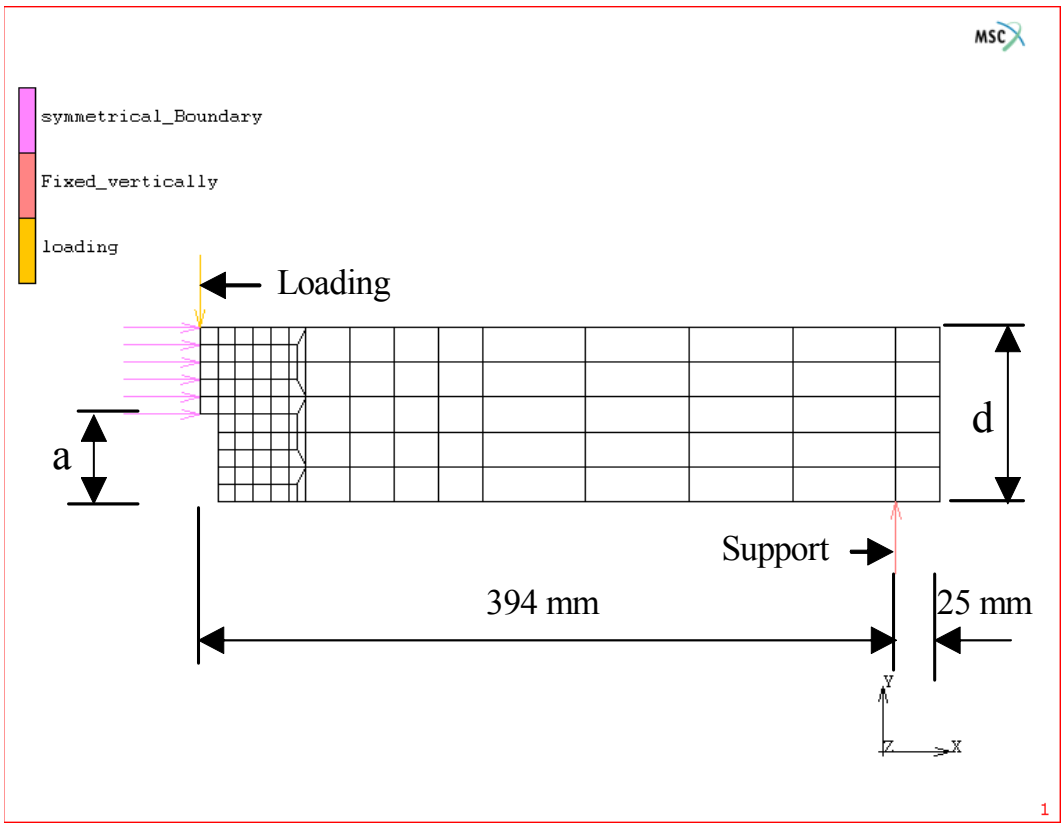

Figure 5.1 - Finite element model (Case 1)

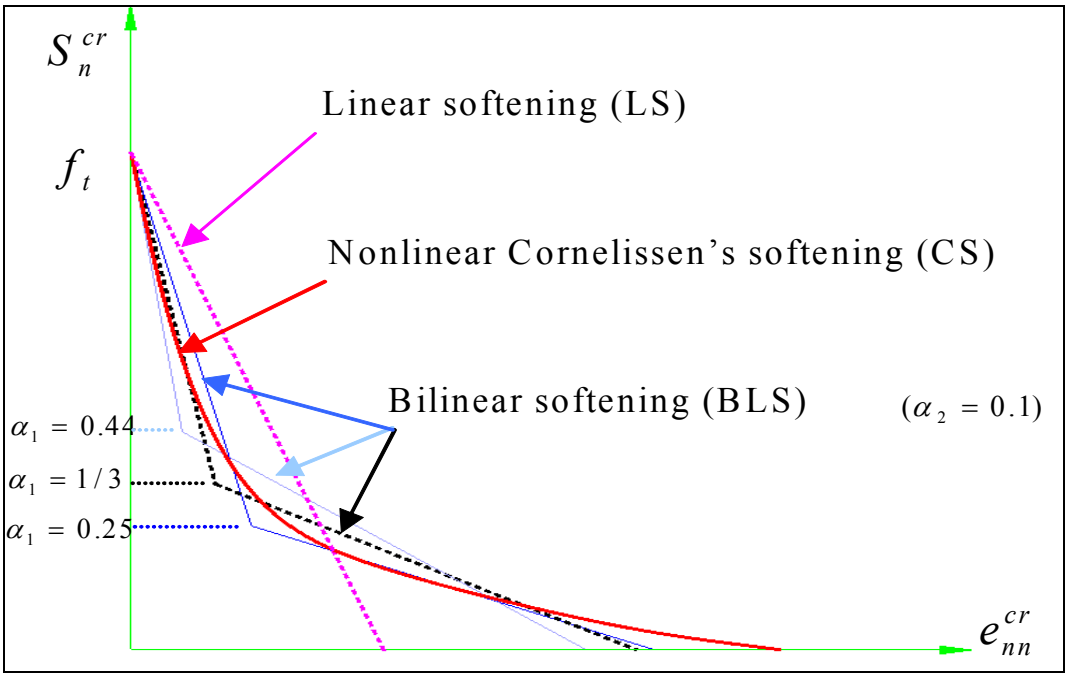

Figure 5.2 - Linear, bilinear and non-linear strain softening

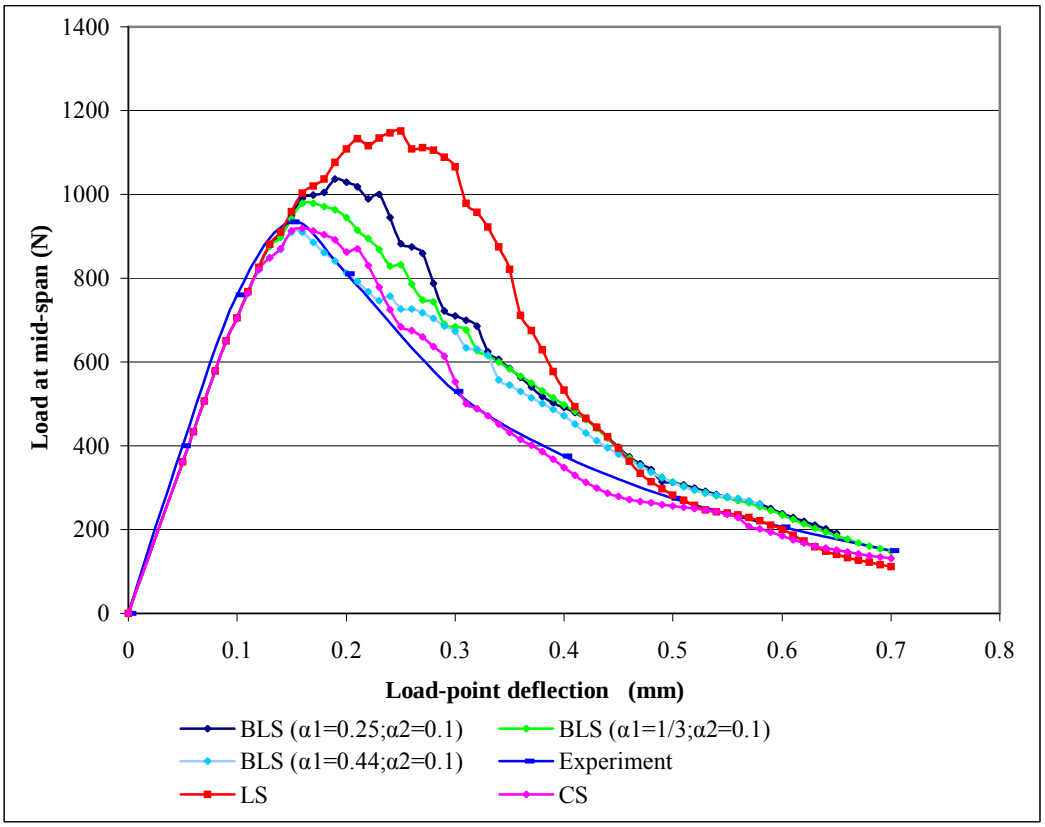

Figure 5.3 - Load-load point deflection for strain-softening branches in Figure 5.2

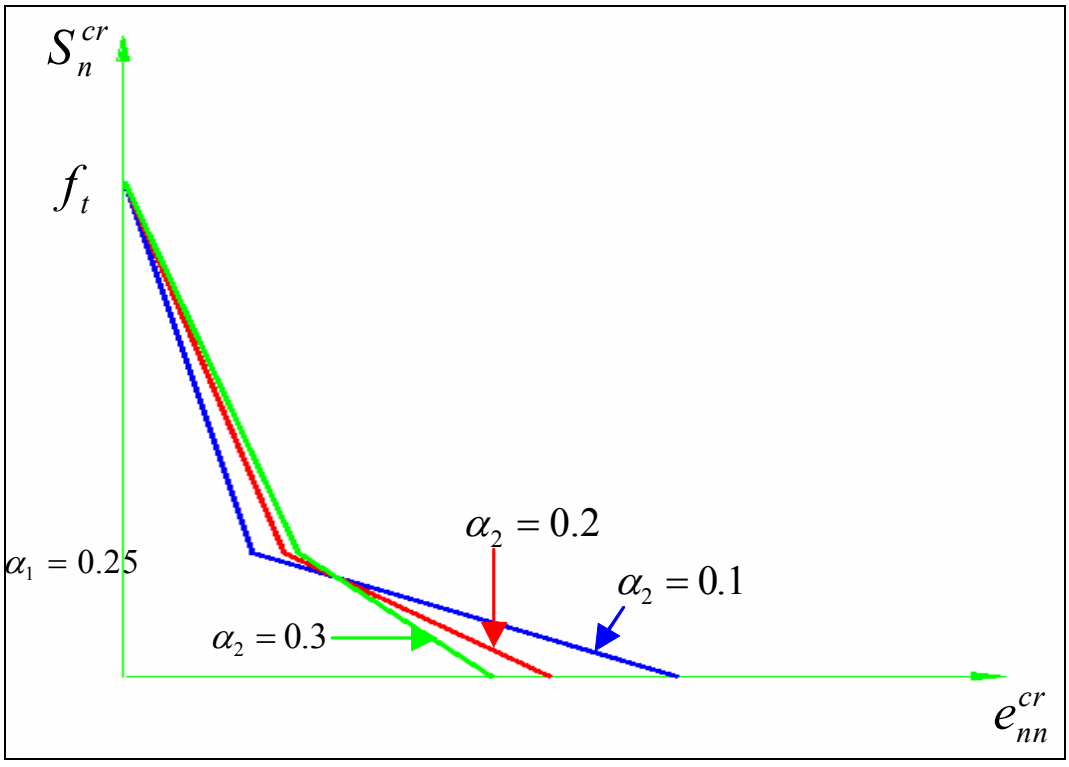

Figure 5.4 - Bilinear strain softening with $\alpha_1 = 0.25$ and $\alpha_2 = 0.1$, 0.2 and 0.3

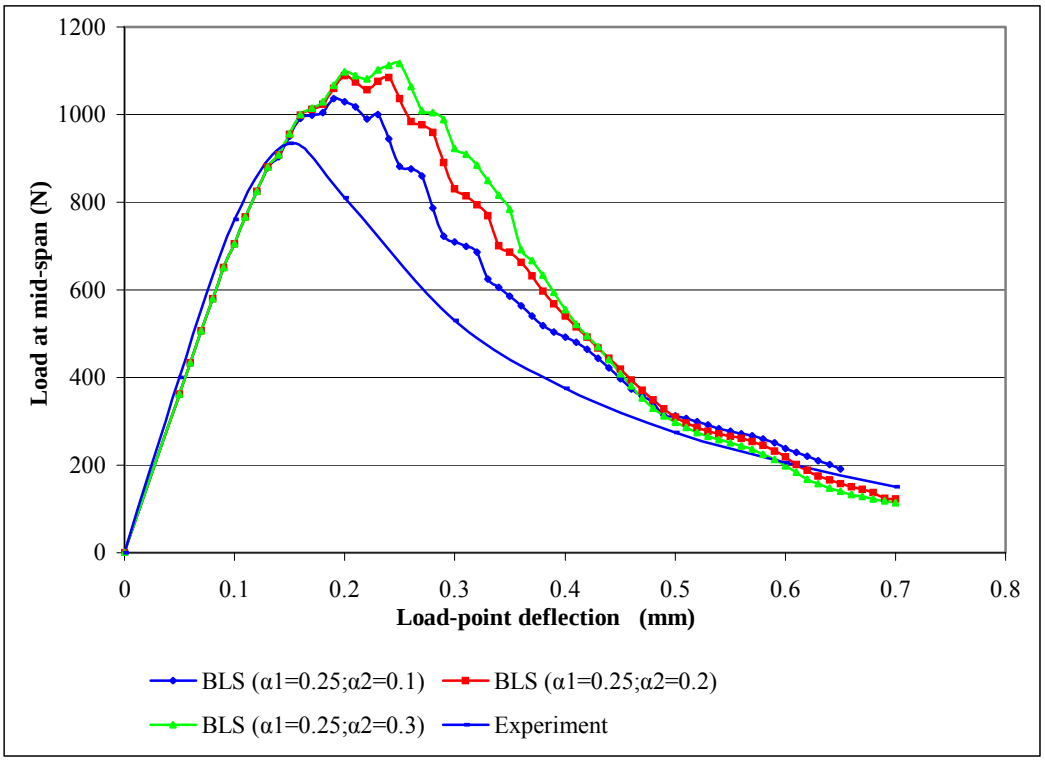

Figure 5.5 - Load-load point deflection for strain-softening branches in Figure 5.4

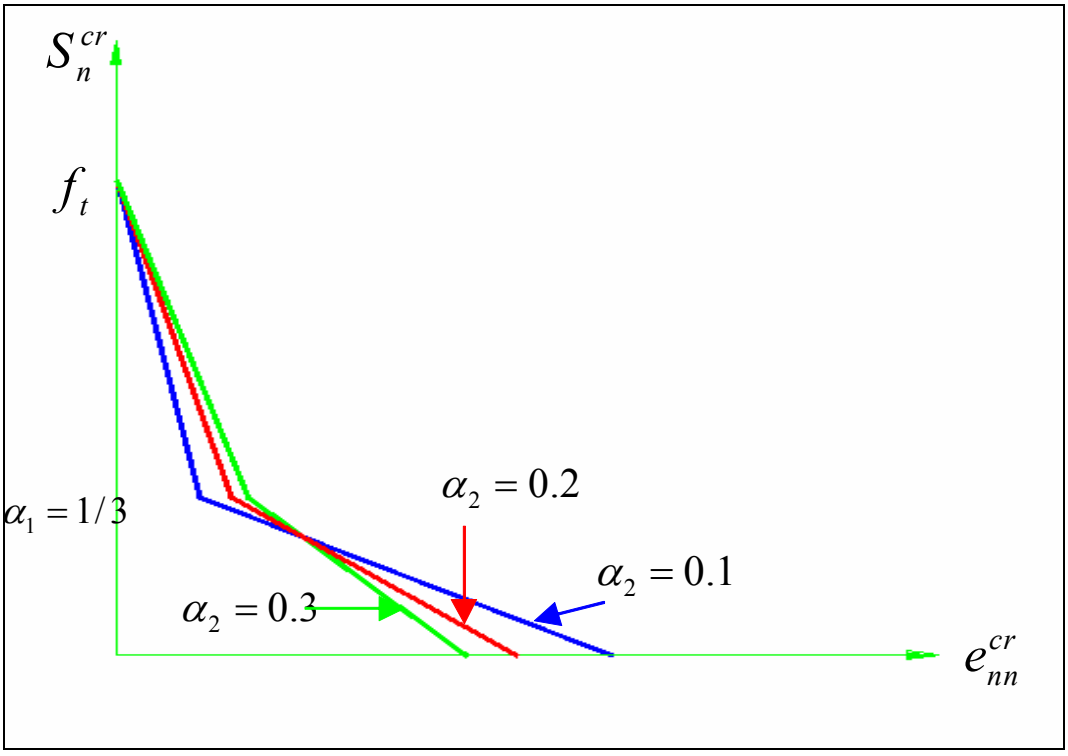

Figure 5.6 - Bilinear strain softening with $\alpha_1 = 1/3$ and $\alpha_2 = 0.1$, 0.2 and 0.3 respectively

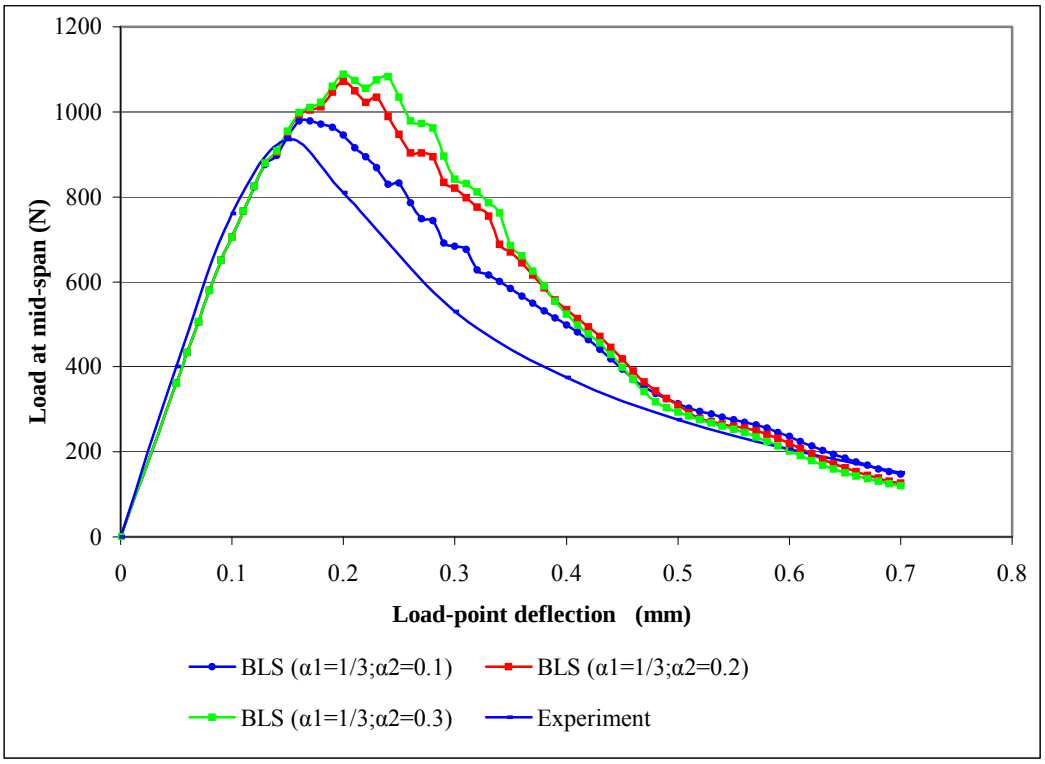

Figure 5.7 - Load-load point deflection for strain-softening branches in Figure 5.6

5.3 Case 2: single-notched shear beam

A single centre-notched shear beam, loaded at points A and B and supported at two points at the bottom, is shown in Figure 5.8. The generality and accuracy of the crack model and the code developed are to be investigated. The beam has been tested experimentally by Arrea & Ingraffea (1981) and is widely used as a benchmark for numerical fracture analysis models (Rots & de Borst 1987; Bhattacharjee & Leger 1994).

The FE model is shown in Figure 5.8 and the material properties and constitutive parameters are as follows.

Young's modulus E = 24 800 MPa; Tensile strength f_t = 2.8 MPa

Poisson's ratio υ = 0.18; Fracture energy G_f = 0.1 N/mm

Thickness of the beam = 156 mm Bilinear shape parameters α_1 = 1/3 and α_2 =0.2

Crack characteristic length h_c = 13.5 mm

During laboratory testing the load was applied to the specimen by means of a stiff steel beam, ACB. Since the steel beam is statically determinate, the ratio between its reactions at A and B (acting on the concrete beam) and the applied load can be easily determined. The load in this study was therefore applied directly to the concrete beam at A and B, using the same ratios as in the laboratory test. The crack opening is measured as a crack mouth sliding displacement (CMSD) and a crack mouth opening displacement (CMOD), as defined in Figure 5.13.

Snap-back behaviour has been modelled numerically by several researchers (Rots & Blaauwendraad 1989; Rots & de Borst 1987; Bhattacharjee & Leger 1994), using an indirect displacement control strategy with the CMSD as controlling parameter. Due to the limitations in the FE package, which lacks the mechanism for an indirect displacement control solution, the author had to resort to a manual solution procedure. A peak load was firstly obtained by identifying the load beyond which the beam experienced unstable cracking and the solution was unable to converge. Subsequently, manual unloading beyond the peak load is achieved by defining the unloading path. It should be noted that the CMSD response of the beam is sensitive to the unloading path, which explains why CMSD was adopted to control the applied load directly or indirectly in the experimental and numerical investigations carried out by other researchers.

Three solutions are presented: two linear softening models (labelled as LS) with $\beta = 0.05$ and 0.1 respectively, and one bilinear softening model with $\beta = 0.05$ (labelled as BLS). A comparison with the experimental results for the load – CMSD response is shown in Figure 5.9. In the post-peak regime, the results of the linear softening model with $\beta = 0.1$ fall outside the range of the experimental results, producing a less accurate post-peak response than the other two solutions. The results of the bilinear softening model are well within the experimental scattering range and show a significant improvement over the linear softening solutions. It is also observed that the CMSD response is very sensitive to the shear-softening parameters selected for this specimen due to the mixed-mode fracture. The numerical results agree well with the results of other researchers.

The load–crack mouth opening displacement (CMOD) response obtained in this study, together with the results from Rots & de Borst (1987) (labelled as R&D 1987), are shown

in Figure 5.11. It must be noted that a mode I fracture energy of 0.1 N/mm is used in this investigation (for the purpose of comparison with other investigations) whereas a fracture energy of 0.075 N/mm was adopted by Rots & de Borst (1987). Most past investigations have adopted a mode I fracture energy of 0.1 N/mm such as Bhattacharjee & Leger (1994) and Rots & Blaauwendraad (1989) and others. For comparison with the results from the more available past investigations (mainly to compare with the work done by Bhattacharjee & Leger 1994), a mode I fracture energy of 0.1 N/mm was also adopted in this research. This is the main reason for the post-peak CMOD response of this investigation being slightly higher than those from Rots & de Borst (1987). In general, however, good agreement has been achieved.

As pointed out by Rots & de Borst (1987), the beam responded in both mode I and II fracture propagations, with mode I being the main fracture mechanism in this application. This is confirmed by the ultimate CMOD response being approximately twice the corresponding CMSD response.

The load-vertical displacement response at point C obtained in this study for the three cases mentioned above, together with the results from Rots & Blaauwendraad (1989) (labelled as R&B 1989) and Bhattacharjee & Leger (1994) (labelled as B&L 1994), are shown in Figure 5.10. The deflection at point C is obtained from the deflections at points A and B by assuming that the steel beam ACB used in the experimental test was infinitely stiff. Good agreement with the results obtained by Rots & Blaauwendraad (1989) and Bhattacharjee & Leger (1994) is exhibited for the snap-back behaviour. A mode I fracture energy of 0.1 N/mm was selected in the latter two references (Rots & Blaauwendraad 1989; Bhattacharjee & Leger 1994).

The final crack zone and the deformed shape of the beam are shown in Figures 5.12 and 5.13. Figure 5.12 demonstrates that there is some discrepancy between the smeared cracks and the crack profile observed in the test. As shown in Figures 5.9 to 5.11, the post-peak structural resistance does not reduce to zero, indicating that stress-locking (which is inherent in smeared crack models) is present. This phenomenon was also observed in the other investigations using smeared crack models (Rots & Blaauwendraad 1989; Bhattacharjee & Leger 1994).

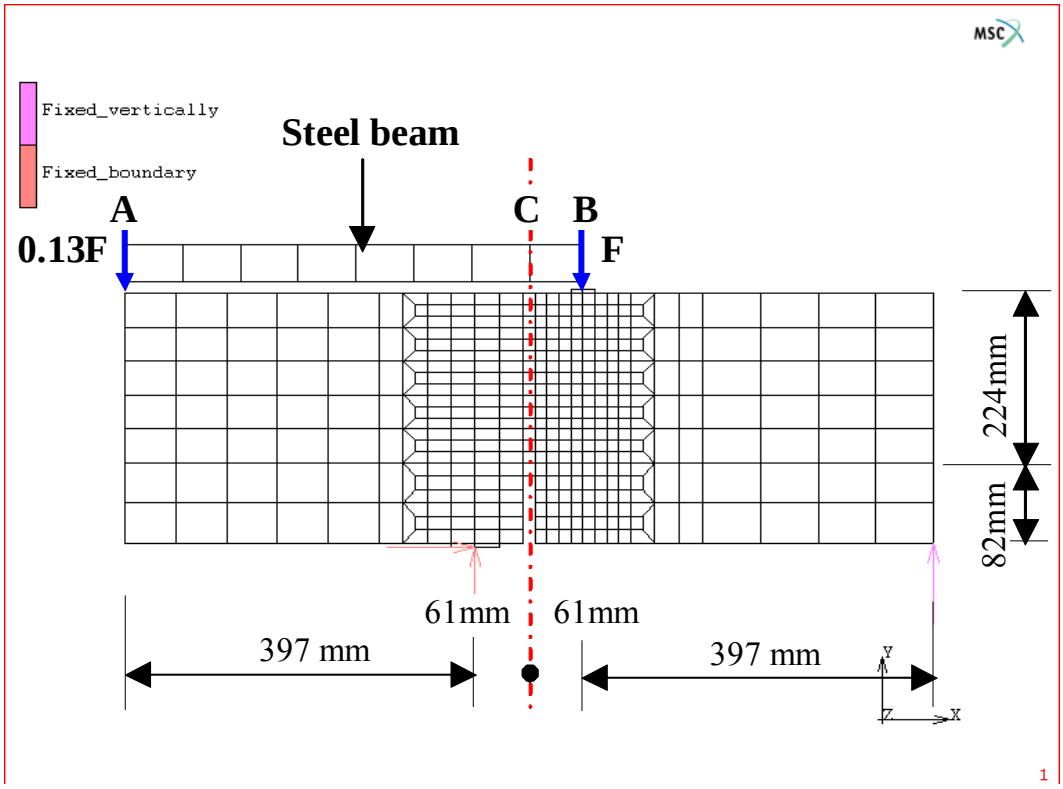

Figure 5.8 - Finite element model (Case 2)

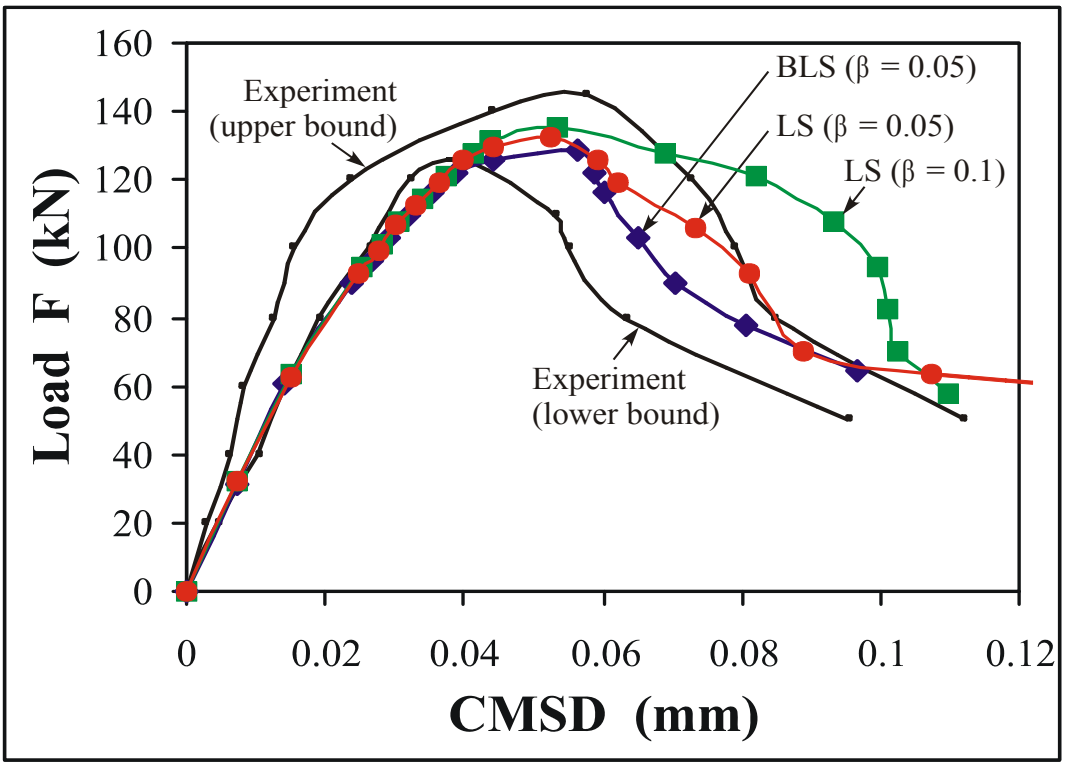

Figure 5.9 - Load – CMSD

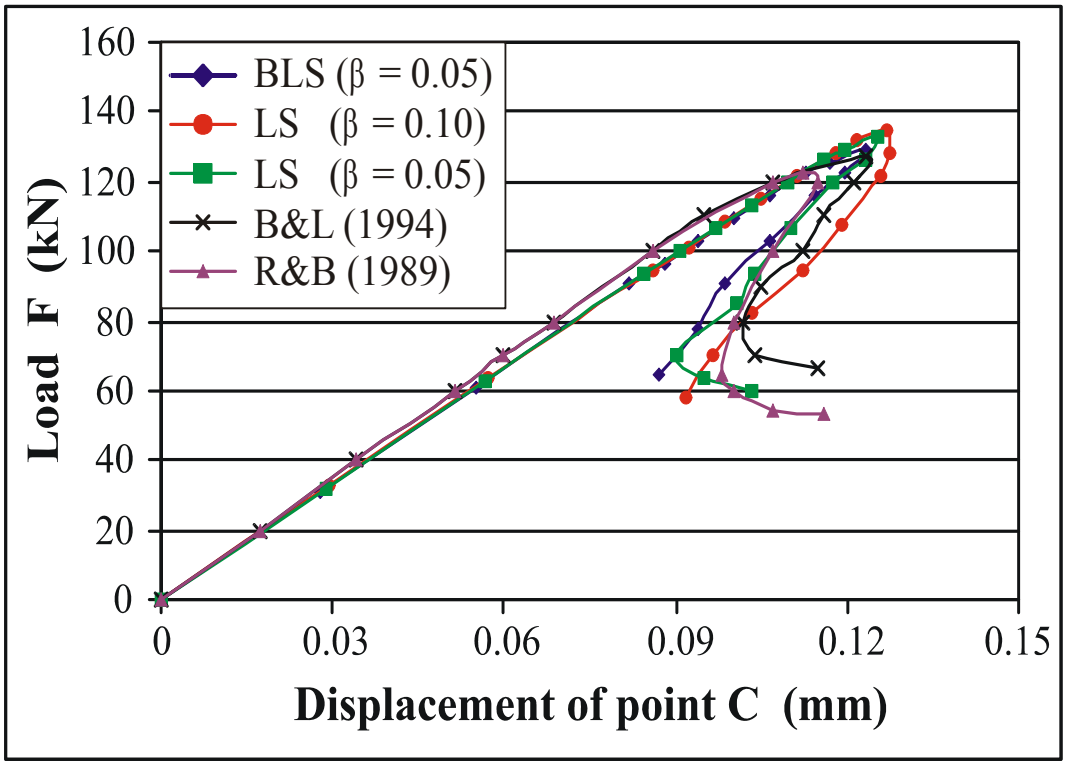

Figure 5.10 - Snap-back in load – deflection at point C

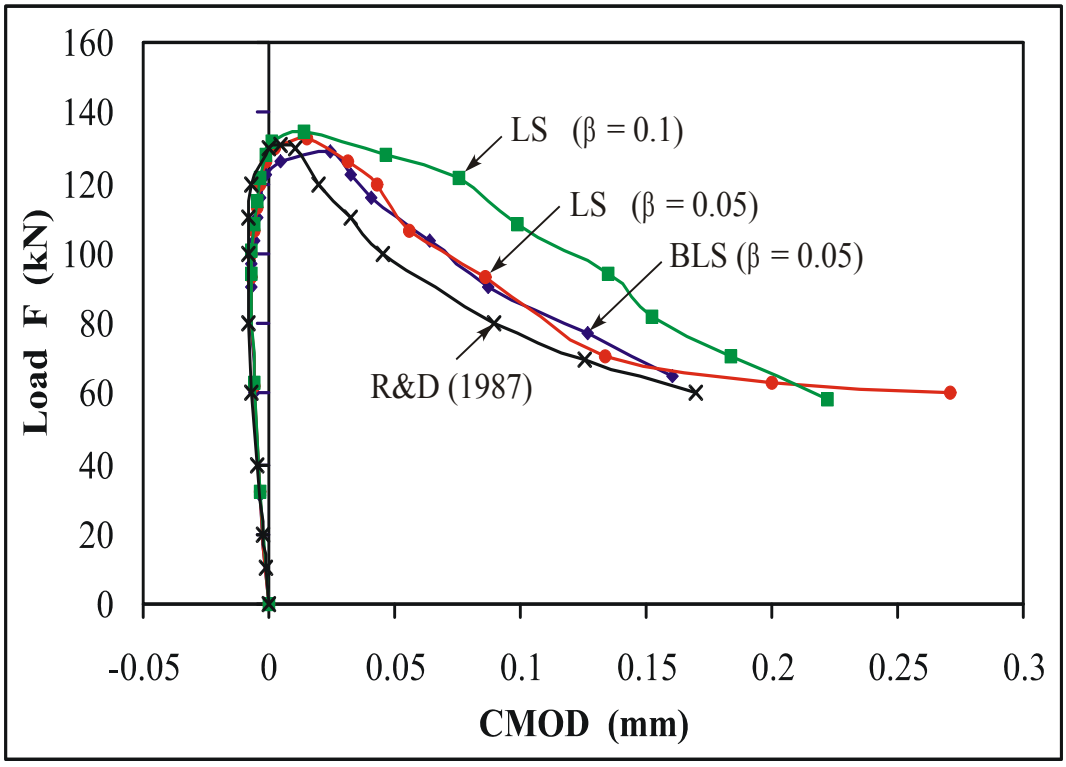

Figure 5.11 - Load – CMOD

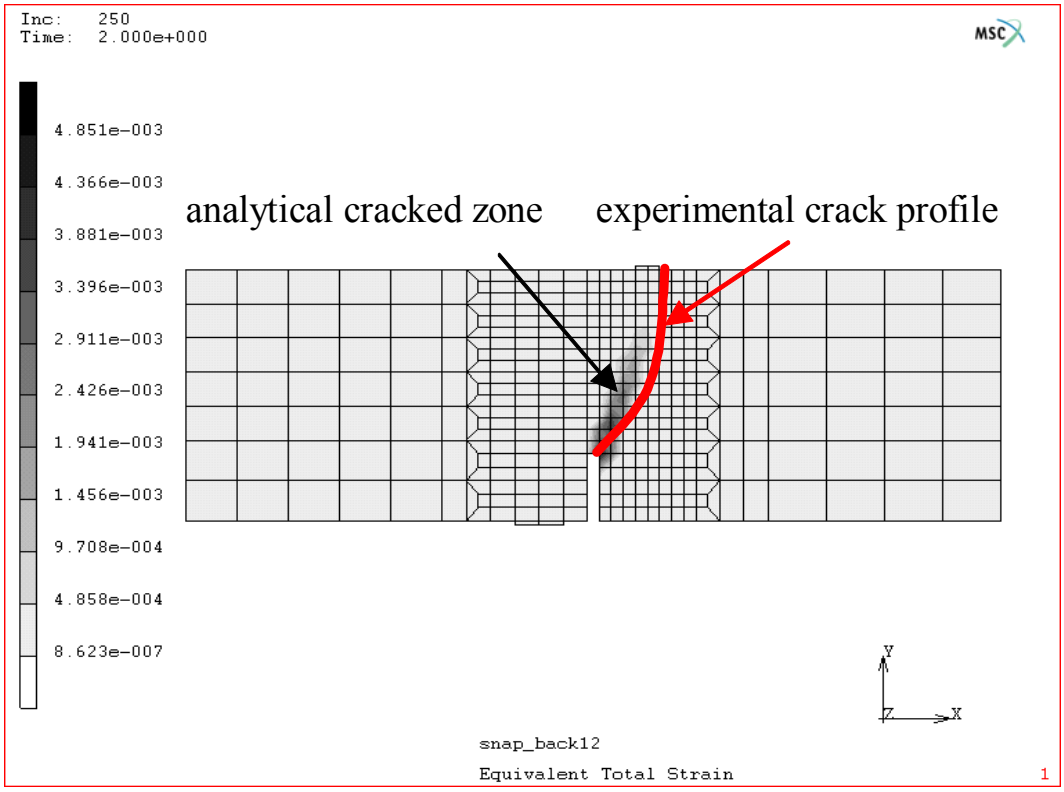

Figure 5.12 - Crack profiles

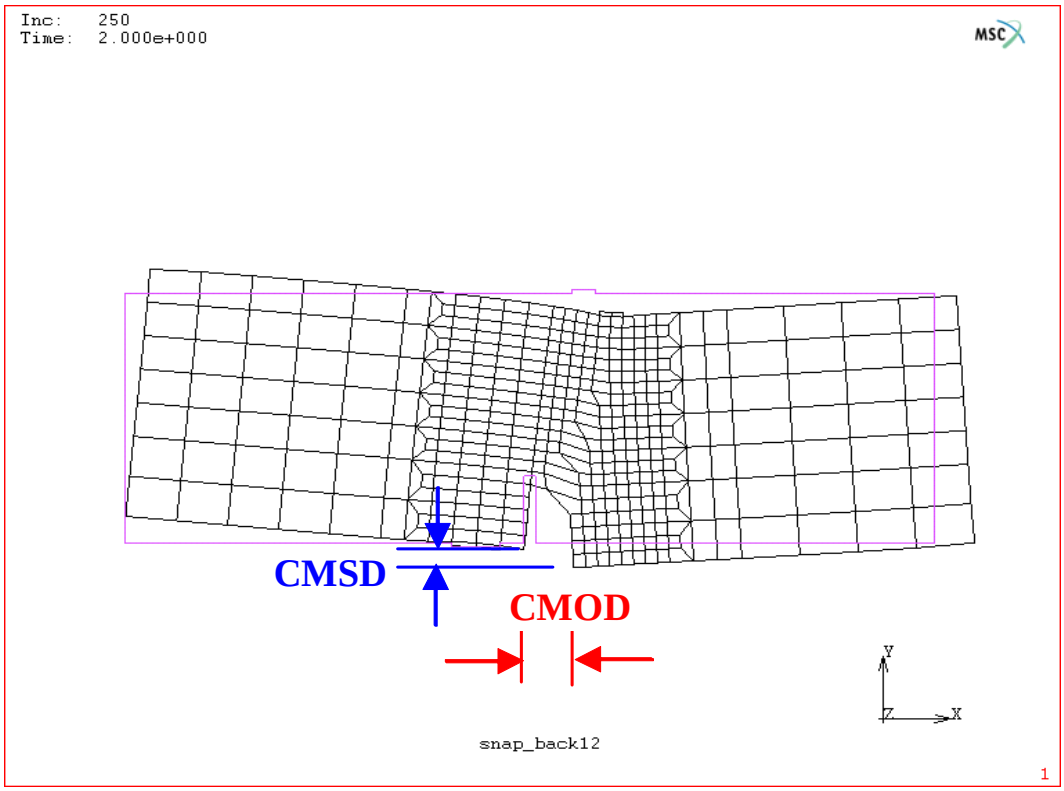

Figure 5.13 - Predicted deformation

5.4 Case 3: mesh objectivity and second-order elements validation

A single-notched, three-point loaded beam is used to validate the mesh objectivity of the FE analysis of concrete fracture and the use of second-order elements for the implementation of the cracking model. This specimen was tested experimentally by Bažant & Pfeiffer (1987) and numerically investigated by Bhattacharjee & Leger (1993).

The material properties are adopted from Bhattacharjee & Leger (1993) and are listed below. The specimen is shown in Figure 5.14. Linear strain softening is selected for comparison purposes. Shear softening does not influence the peak load in this specific application in which mode I fracture propagation is dominant.

Young's modulus E = 27 413 MPa;	Tensile strength f_t = 2.886 MPa
Poisson's ratio υ = 0.18;	Fracture energy G_f = 0.04029 N/mm
Thickness of beam = 38.1 mm;	Depth of beam d = 304.8 mm

The crack characteristic length h_c is dependent on the size of the elements at the crack in the different FE models used.

Three FE models with 6, 12 and 24 elements through the depth of the beam are created for the mesh objectivity study, as shown in Figures 5.15 to 5.17 (namely model 1). The three FE models in Figures 5.15 to 5.17 are also modelled by the eight-noded, second-order elements with full integration for the purpose of verifying the crack models implemented with high-order elements.

The loads P_0 required to cause a crack-tip tensile stress equal to the tensile strength f_t are determined using elastic bending theory and are given in Table 5.1 for the three FE models. The peak loading resistances P_u from the analyses for each of the three FE models are also shown in Table 5.1. Figure 5.18 compares the experimental results, the conventional elasto-brittle strength-based fracture analysis (labelled as SBM) and the numerical analysis done by Bhattacharjee and Leger (1993) (labelled as B&L 1993), by plotting the $\frac{P_u}{P_0}$ ratio versus the mesh fineness. Also shown in Figure 5.18 are the results

from this research (labelled as LS), which appear to be mesh objective since the fineness of the mesh has practically no influence on the predicted response, unlike the SBM analyses. The difference in results between the strain-softening models and the experimental findings, as explained by Bhattacharjee and Leger (1993), stems from the fact that the constitutive model parameters had to be assumed since they were not available from the experimental results.

The peak loading resistance P_u from the analyses of the three FE models of the second-order elements and the related $\frac{P_u}{P_0}$ ratio are shown in Table 5.2.

The results from the first-order element models and the second-order element models for the three different mesh finenesses in Figures 5.15 to 5.17 are compared in Figure 5.19. It is clear that the analyses based on the implemented crack models are objective with regard to the different order elements used.

TABLE 5.1 - Loads from elastic bending theory and FE analyses for different mesh finenesses – first-order elements

Mesh fineness (number of elements through the depth)	P_0 **(kN)**	P_u **(kN)**	$\frac{P_u}{P_0}$
Coarse mesh – 6 elements	6.65	7.304	1.098
Medium mesh – 12 elements	6.42	7.064	1.100
Fine mesh – 24 elements	6.31	6.936	1.099

TABLE 5.2 - Loads from elastic bending theory and FE analyses for different mesh finenesses – second-order elements

Mesh fineness (number of elements through the depth)	P_0 **(kN)**	P_u **(kN)**	$\frac{P_u}{P_0}$
Coarse mesh – 6 elements	6.65	7.330	1.102
Medium mesh – 12 elements	6.42	7.036	1.096
Fine mesh – 24 elements	6.31	6.860	1.087

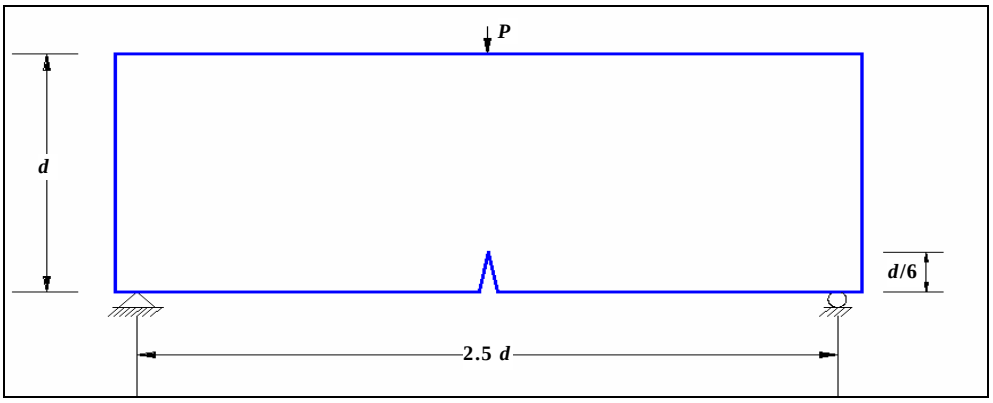

Figure 5.14 - Geometric configurations and boundary conditions

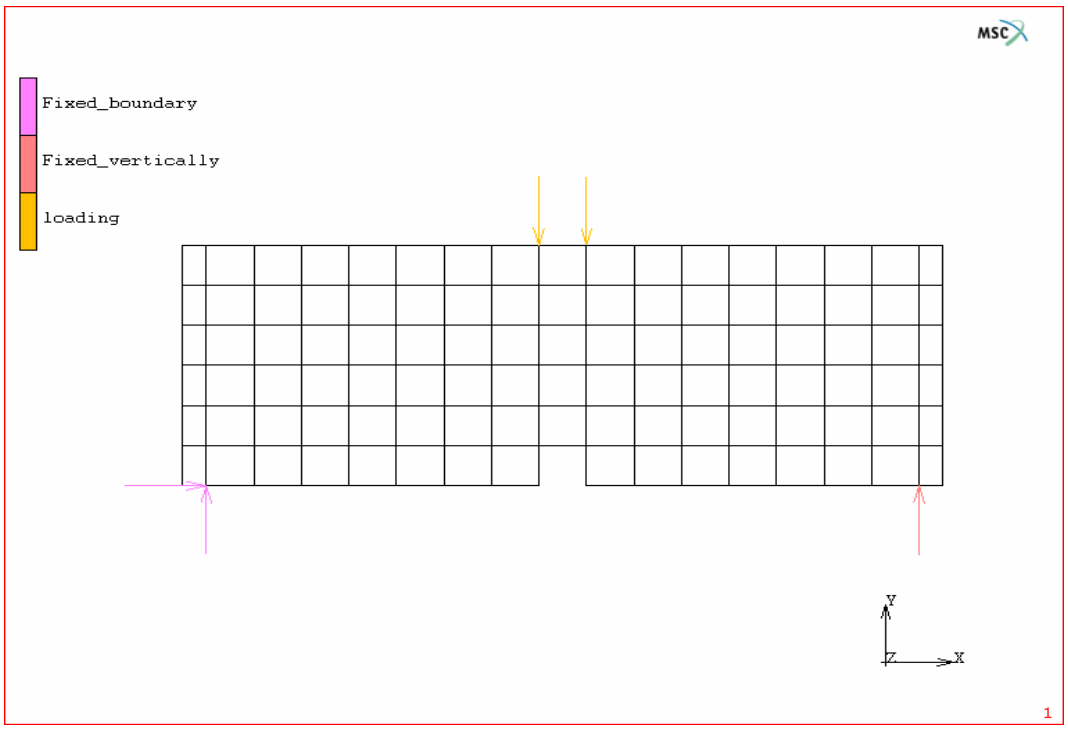

Figure 5.15 - Coarse model 1 – 6 elements in depth

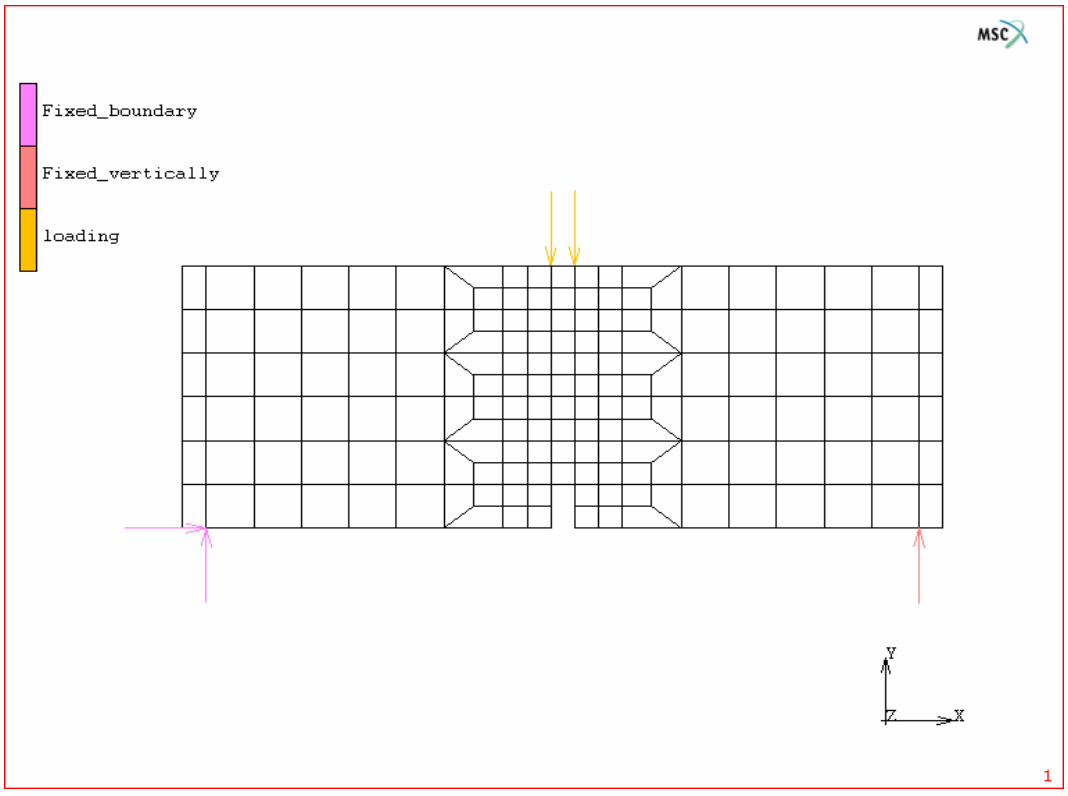

Figure 5.16 - Medium model 1 – 12 elements in depth

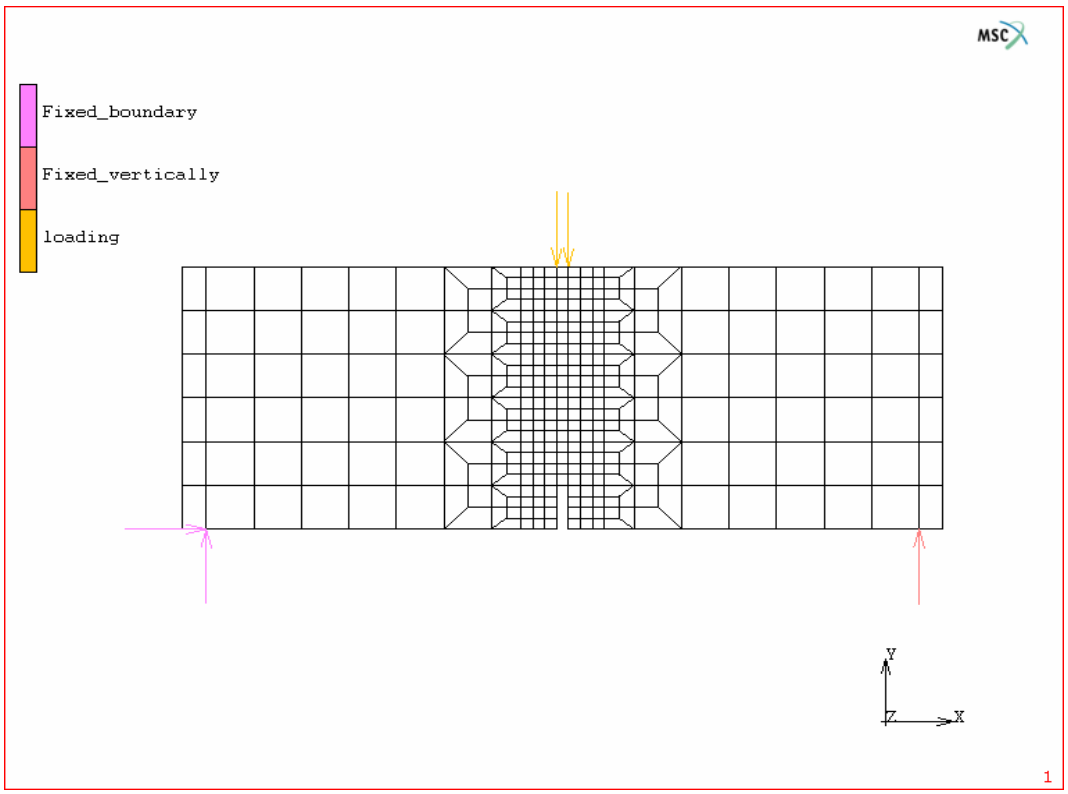

Figure 5.17 - Fine model 1 – 24 elements in depth

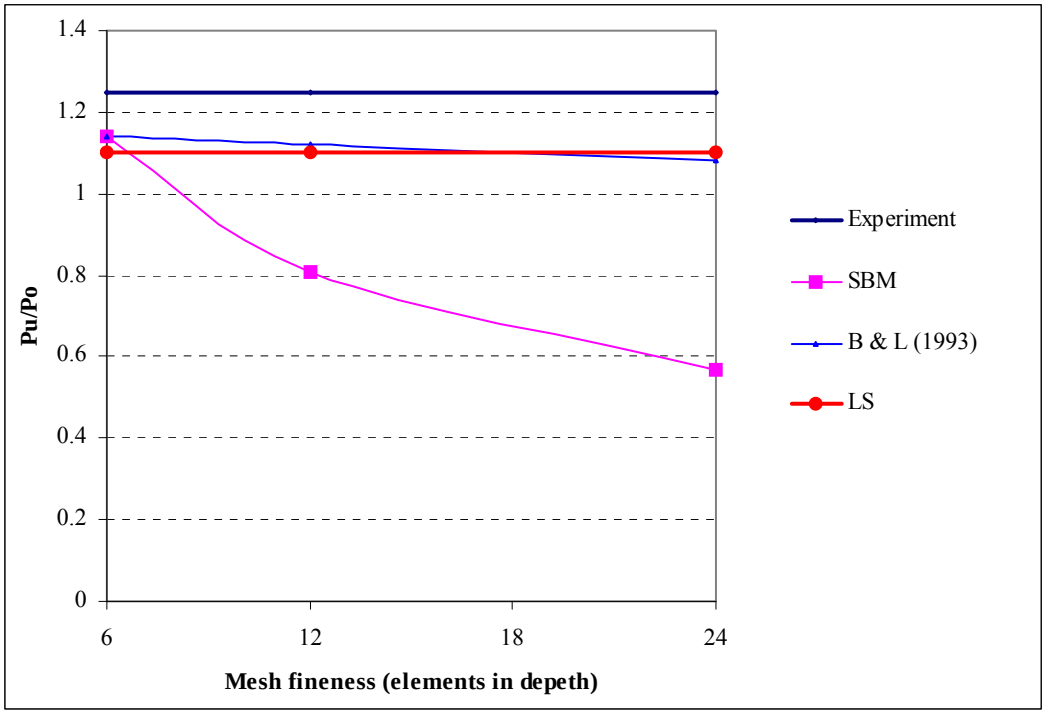

Figure 5.18 - Comparison of mesh objectivity (models 1)

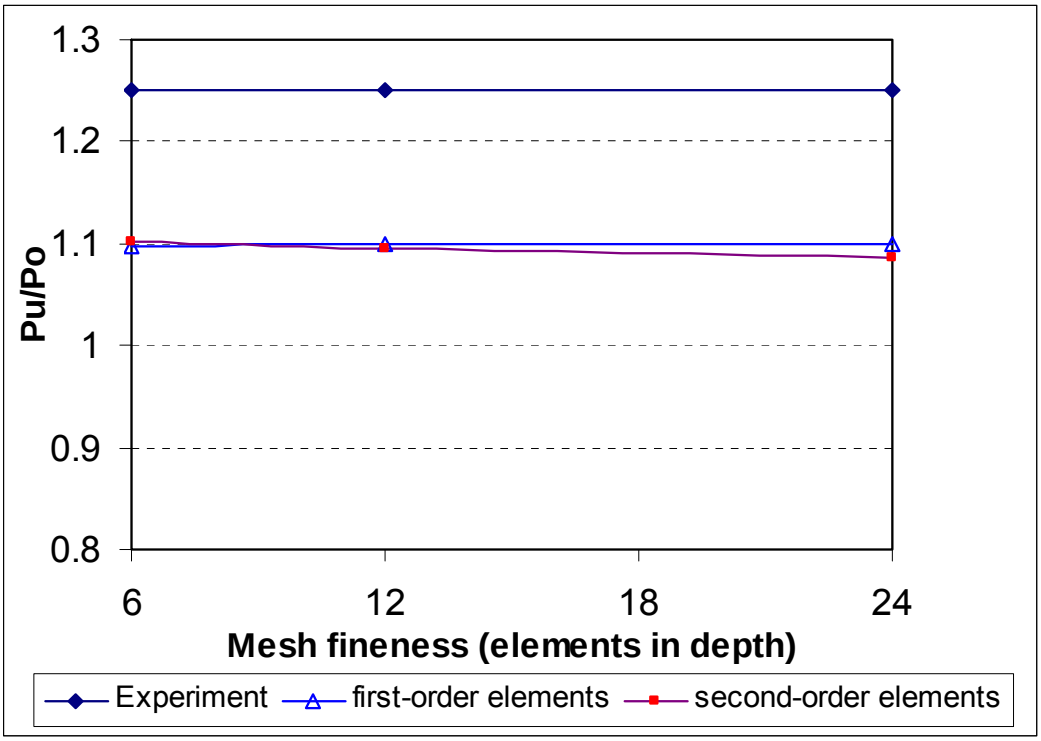

Figure 5.19 - Comparison of element objectivity (models 1)

The above mesh objectivity verification analyses have the following limitations:

- The width of the notch in the three meshes is not fixed but varies with the element size used in the mesh.
- The loadings in the three mesh models are not applied at the same distance to the centreline of the models, but vary with the element size used.

Therefore, a further mesh objectivity study was carried out to eliminate the above-mentioned limitations. The following three mesh models (namely model 2) (see Figures 5.20 to 5.22) are created in this study based on the same beam configurations. All the material properties and boundary conditions are the same as above. The only difference between these three mesh models (Figures 5.20 to 5.22) and those in the previous mesh objectivity study (Figures 5.15 to 5.17) is that the position of the loadings and the width of the notches are kept the same in order to achieve the aim of this mesh objectivity verification.

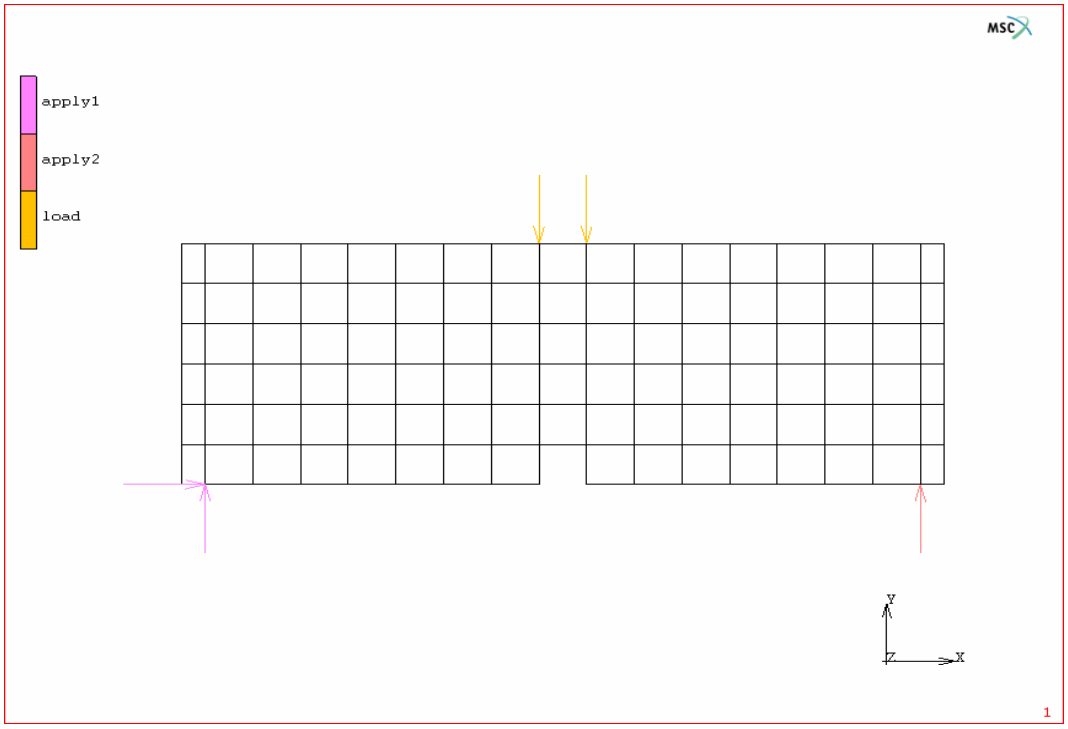

Figure 5.20 - Coarse model 2 – 6 elements in depth

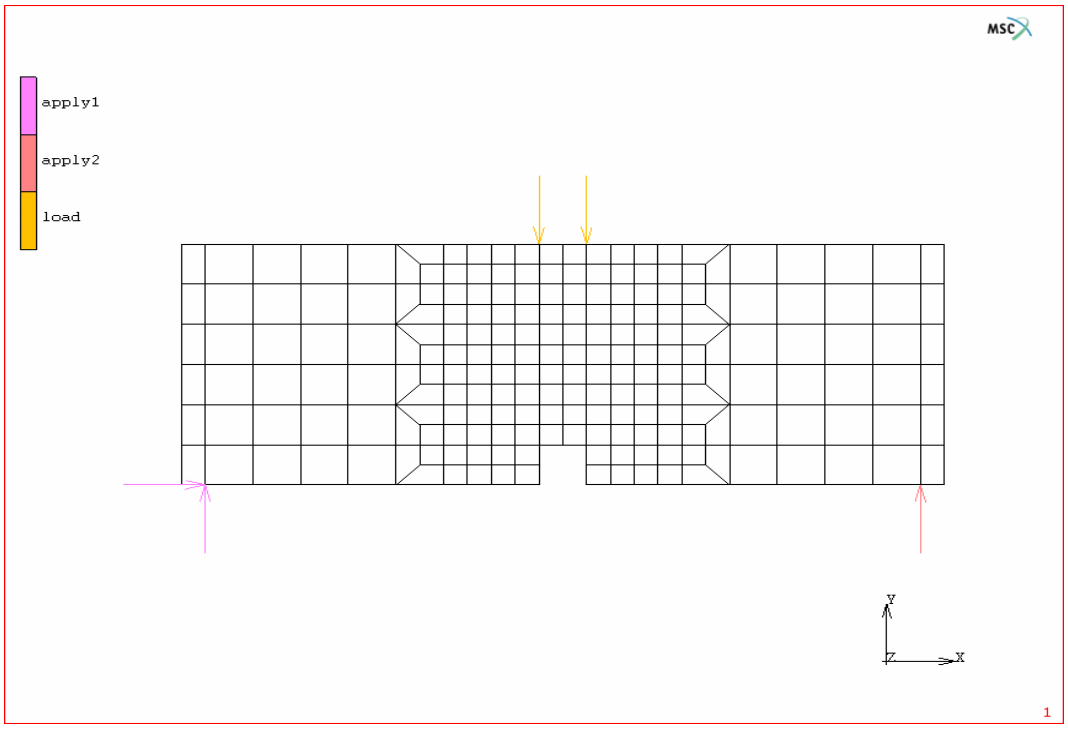

Figure 5.21 - Medium model 2 – 12 elements in depth

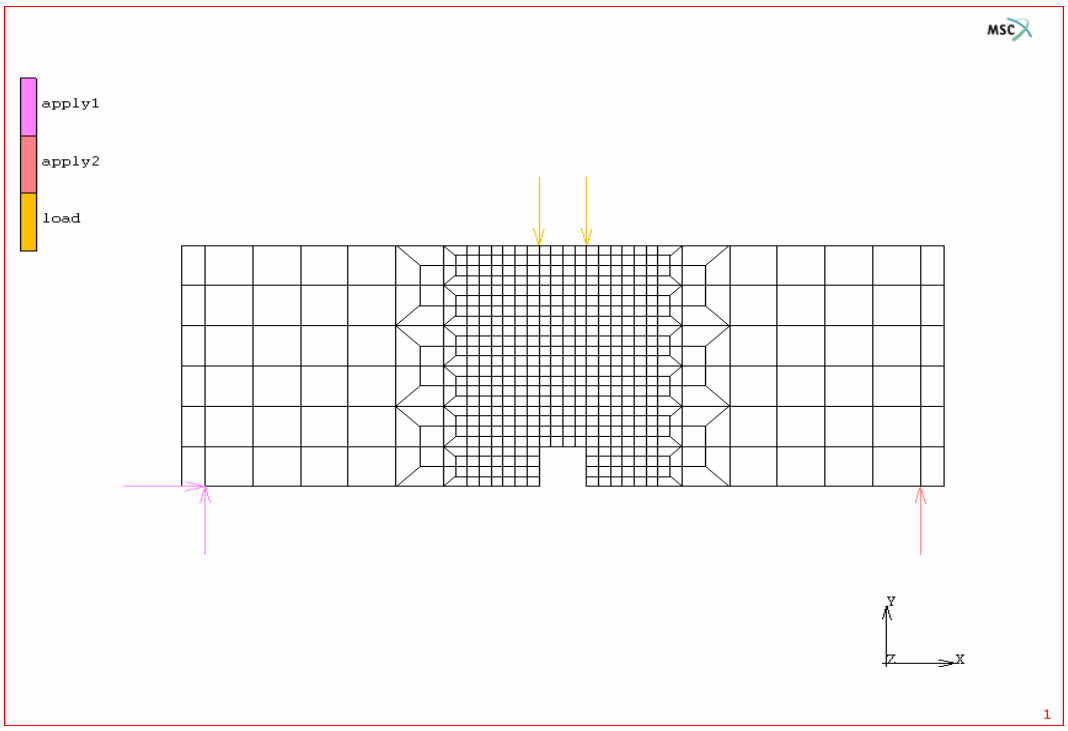

Figure 5.22 - Fine model 2 – 24 elements in depth

The results of the analyses are shown in Figure 5.23 in which it can be seen that the crack analysis method and procedures developed can be regarded as mesh objective. Different meshes only result in a maximum discrepancy of approximately 7% in the result of the $\frac{P_u}{P_0}$ ratio.

It can be concluded from the verification studies on mesh objectivity that the proposed crack model and the numerical technique developed achieve the goal of mesh objectivity.

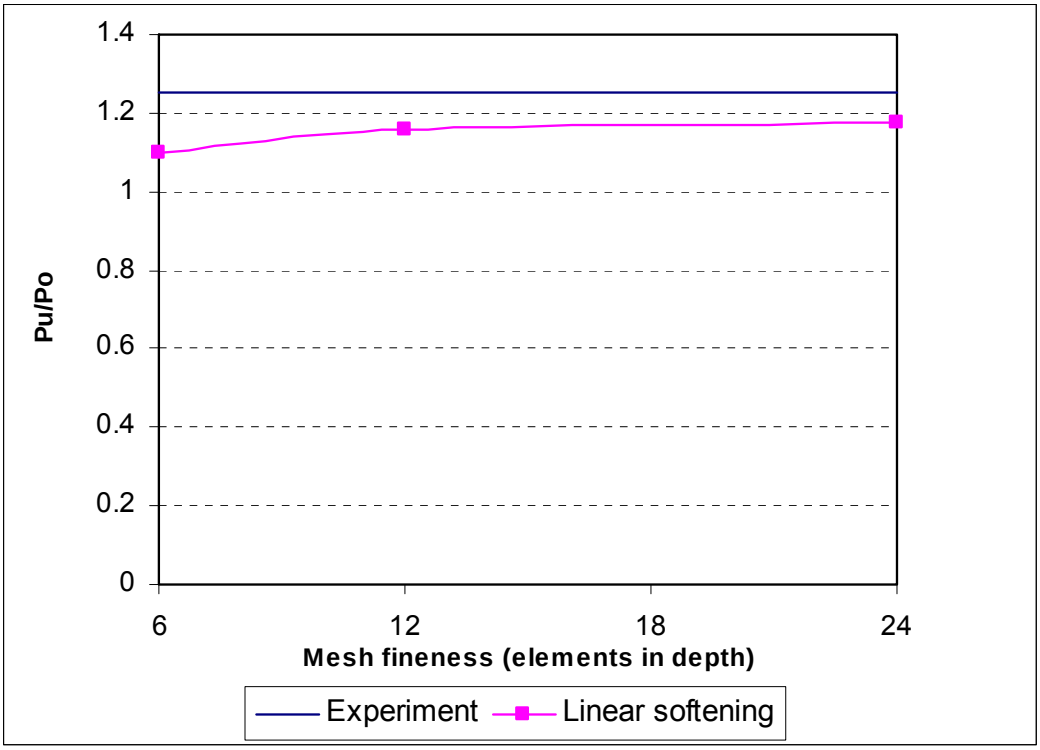

Figure 5.23 - Comparison of mesh objectivity (models 2)

5.5 Conclusion

In this chapter, a comprehensive study on the versatility and accuracy of implementation of the proposed smeared crack FE model, based on non-linear fracture mechanics for concrete structures, has been carried out for the purpose of eventually applying the constitutive model in predicting the crack behaviour of concrete dams and in evaluating dam safety.

A three-point, single-notched beam was considered for the comparative study on linear, bilinear and non-linear experimental curved softening, with experimental load-deflection relationships. The parametric bilinear shape study shows that if α_1 and α_2 are set in the vicinity of 1/3 and 0.1 respectively, which is a good approximation to the experimental non-linear softening curve of Cornelissen *et al*. (1986), very good numerical results are obtained compared with the results of the experiment. It can be concluded that a bilinear softening analysis yields significantly better results than the linear softening solutions mostly adopted in concrete cracking analysis, and that it can be applied with confidence in the fracture analysis of concrete structures.

Normal and shear stress field prevailingly exists in concrete structures. Therefore, it is very important to validate the adopted numerical procedure in mixed mode application. A mixed-mode fracturing beam were analysed with the results demonstrating that bilinear mode I softening is superior to the linear strain softening.

The mesh and element-order objectivity of the numerical method developed was observed in the analysis of a three-point, single-notched beam.

Based on these case studies, the following conclusions are drawn:

- The crack model is valid for both mode I and mixed-mode fracture analysis.
- The proposed bilinear softening model remains relatively simple to implement, but significantly improves the prediction of the softening response.
- The proposed method is mesh objective and could overcome problems such as non-convergence and snap-back.
- The proposed method is element-order objective.